The Inositol Trisphosphate Receptor (IP_3R) is Dispensable for Rotavirus-induced Ca^{2+} Signaling and Replication but Critical for Paracrine Ca^{2+} Signals that Prime Uninfected Cells for Rapid Virus Spread

Jacob L. Perry, Francesca J. Scribano, John T. Gebert, Kristen A. Engevik, Jenna M. Ellis, and Joseph M. Hyser

Alkek Center for Metagenomic and Microbiome Research; Department of Molecular Virology and Microbiology, Baylor College of Medicine, Houston, TX, USA.

Running title: Ca^{2+} waves prime nearby cells for rotavirus spread

*Correspondence should be sent to:

Joseph M. Hyser

Joseph.Hyser@bcm.edu

No conflicts of interest exist.

Abstract

Rotavirus is a leading cause of viral gastroenteritis. A hallmark of rotavirus infection is an increase in cytosolic Ca^{2+} caused by the nonstructural protein 4 (NSP4). NSP4 is a viral ion channel that releases Ca^{2+} from the endoplasmic reticulum (ER) and the increase in Ca^{2+} signaling is critical for rotavirus replication. In addition to NSP4 itself, host inositol 1,4,5-trisphosphate receptor (IP_3R) ER Ca^{2+} channels may contribute to rotavirus-induced Ca^{2+} signaling and by extension, virus replication. Thus, we set out to determine the role of IP_3R Ca^{2+} signaling during rotavirus infection using IP_3R-knockout MA104-GCaMP6s cells (MA104-GCaMP6s-IP_3R-KO), generated by CRISPR/Cas9 genome editing. Live Ca^{2+} imaging showed that IP_3R-KO did not reduce Ca^{2+} signaling in infected cells but eliminated rotavirus-induced intercellular Ca^{2+} waves (ICWs) and therefore the increased Ca^{2+} signaling in surrounding, uninfected cells. Further, MA104-GCaMP6s-IP_3R-TKO cells showed similar rotavirus susceptibility, single-cycle replication, and viral protein expression as parental MA104-GCaMP6s cells. However, MA104-GCaMP6s-IP_3R-TKO cells exhibited significantly smaller rotavirus plaques, decreased multi-round replication kinetics, and delayed virus spread, suggesting that rotavirus-induced ICW Ca^{2+} signaling stimulates virus replication and spread. Inhibition of ICWs by blocking the P2Y1 receptor also resulted in decreased rotavirus plaque size. Conversely, exogenous expression of P2Y1 in LLC-MK2-GCaMP6s cells, which natively lack P2Y1 and rotavirus ICWs, rescued the generation of rotavirus-induced ICWs and enabled plaque formation. In conclusion, this study shows that NSP4 Ca^{2+} signals fully support rotavirus replication in individual cells; however, IP_3R is critical for rotavirus-induced ICWs and virus spread by priming Ca^{2+}-dependent pathways in surrounding cells.

39 **Importance**

40 Many viruses exploit host Ca^{2+} signaling to facilitate their replication; however, little is known
41 about how distinct types of Ca^{2+} signals contribute to the overall dysregulation of Ca^{2+} signaling
42 or promote virus replication. Using cells lacking IP_3R, a host ER Ca^{2+} channel, we could
43 differentiate between intracellular Ca^{2+} signals within virus-infected cells and intercellular Ca^{2+}
44 waves (ICWs), which increase Ca^{2+} signaling in neighboring, uninfected cells. In infected cells,
45 IP_3R was dispensable for rotavirus-induced Ca^{2+} signaling and replication, suggesting the
46 rotavirus NSP4 viroporin supplies these signals. However, IP_3R-mediated ICWs increase
47 rotavirus replication kinetics and spread, indicating that the Ca^{2+} signals from the ICWs may
48 prime nearby uninfected cells to better support virus replication upon eventual infection. This
49 “pre-emptive priming” of uninfected cells by exploiting host intercellular pathways in the vicinity
50 of virus-infected cells represents a novel mechanism for viral reprogramming of the host to gain
51 a replication advantage.

52

53 **Introduction**

54 Calcium (Ca^{2+}) signaling is a cornerstone of cellular communication and is critical for
55 maintaining homeostasis and responding to damage or infection(1). As such, it is unsurprising
56 that many viruses have evolved strategies to exploit these pathways to facilitate virus replication
57 and spread (2). However, the highly interconnected nature of Ca^{2+} signaling has made it
58 challenging to understand how viral and host proteins interact to orchestrate the patterns of Ca^{2+}
59 dysregulation that are observed during infection. One key strategy for virus-induced calcium
60 dysregulation is the expression of viral ion channels, or viroporins, which can conduct Ca^{2+}
61 across host cell membranes (3). The rotavirus nonstructural protein 4 (NSP4) is among the most
62 well-characterized Ca^{2+} conducting viroporins and rotavirus has become a leading model system
63 to study how viruses exploit Ca^{2+} signaling to promote their replication (4). Yet, the interplay
64 between rotavirus- and host-induced Ca^{2+} signaling pathways remain incompletely
65 characterized.

66 Numerous studies show that NSP4 elevates cytosolic Ca^{2+} levels during infection (5-7).
67 NSP4 is a multifunctional endoplasmic reticulum (ER), transmembrane glycoprotein (8, 9) that
68 increases the Ca^{2+} permeability of the ER by forming a Ca^{2+} permeable viral ion channel
69 (viroporin) (10, 11). The NSP4-mediated release of ER Ca^{2+} in turn activates a host process
70 known as store-operated calcium entry (SOCE) to further elevate cytosolic Ca^{2+} levels (12). This
71 is critical for multiple steps in rotavirus replication, including the activation of the autophagy
72 pathway and assembly of the rotavirus outer capsid protein, VP7 (12, 13). Yet, NSP4 may play
73 both a direct and an indirect role in ER Ca^{2+} release, through interaction with host channels. The
74 two main eukaryotic ER Ca^{2+} release channels are the ryanodine receptor (RyR) and the inositol-
75 1,4,5-trisphosphate receptor (IP_3R), and while RyR expression is generally restricted to excitable
76 cells, IP_3R is widely expressed in most cell types (14). Mammals have three IP_3R genes, each
77 with multiple splice variants that provides nuance to the regulation of IP_3R Ca^{2+} release and

78 therefore the ability to shape Ca^{2+} signals (14, 15). The IP_3R channel is activated by IP3 and
79 channel opening is regulated by cytosolic Ca^{2+} in a biphasic manner, such that low cytosolic
80 Ca^{2+} levels potentiates ER Ca^{2+} release and increasing cytosolic Ca^{2+} levels inhibit ER Ca^{2+}
81 release (16). Thus, even though the NSP4 viroporin directly alters ER and cytosolic Ca^{2+}, NSP4
82 Ca^{2+} release may also potentiate IP_3R activity, increasing the Ca^{2+} dysregulation of host cells.

83 In addition to NSP4 and IP_3R crosstalk within infected cells, we recently discovered that
84 rotavirus infection triggers intercellular Ca^{2+} waves (ICWs) through the release of ADP from
85 infected cells and activation of P2Y1 purinergic receptors on neighboring cells. Activation of
86 P2Y1 receptors results in an IP_3R-mediated ER Ca^{2+} signal and since many ICWs are produced
87 during infection, this significantly increases Ca^{2+} signaling in neighboring, uninfected cells as
88 well (17). Thus, the ER Ca^{2+} store is a critical source of Ca^{2+} signals in both rotavirus infected
89 and the nearby uninfected cells and IP_3R has the potential to significantly impact the overall
90 landscape of rotavirus induced Ca^{2+} signaling dysregulation.

91 Thus, the goal of this study is to examine the contribution of IP_3R to rotavirus Ca^{2+}
92 dysregulation and by extension, its role in rotavirus infection, replication and spread. While
93 HEK293 and HeLa cells with genetic knockout of all three IP_3R genes (e.g., IP_3R1, IP_3R2, and
94 IP_3R3) have been established previously, these cell lines are suboptimal for studying rotavirus
95 replication and it is not known whether they support the rotavirus ICW signaling pathway (15,
96 18). Thus, we generated an IP_3R triple knockout in MA104 cells, a vervet monkey (*Chlorocebus*
97 *pygerythrus*) kidney cell line commonly used to study rotavirus (17, 19, 20). We found that IP_3R
98 was not necessary for aberrant Ca^{2+} signaling in infected cells, but was necessary for Ca^{2+}
99 dysregulation in neighboring, uninfected cells. In parallel, IP_3R was dispensable for single-round
100 rotavirus infection and replication, but lack of IP_3R, and therefore lack of ICW signaling, strongly
101 reduced rotavirus spread. This study provides new insights into mechanisms exploited by

102 viruses to reprogram infected cells but also to pre-program surrounding cells for subsequent
103 rounds of infection.
104

105 **Materials and Methods**

106 **Cells and viruses.**

107 All cells were cultured in complete DMEM [high glucose DMEM supplemented with 10% fetal
108 bovine serum (FBS) and Antibiotic/Antimycotic (Invitrogen)] and incubated at 37°C in 5% CO_2.
109 HEK293 and HEK293-IP_3R-TKO cells were provided by Dr. David Yule (15, 21). The MA104
110 (vervet monkey kidney), LLC-MK2 (rhesus monkey kidney), HEK293 and HEK293-IP_3R-TKO
111 cell lines were engineered to express the cytosolic Ca^{2+} sensor, GCaMP6s, as previously
112 described (20, 22). All rotavirus infections were at the indicated MOI for 1 hr with a recombinant
113 SA11 expressing mRuby3 from gene 7 (SA11-mRuby), which was propagated as previously
114 described (20, 23).

115 **MA104-GCaMP6s-IP_3R triple-knockout generation.**

116 *CRISPR/Cas9 development and transduction*

117 MA104 cells lacking IP_3R expression (MA104-GCaMP6s-IP_3R-TKO) were generated by
118 lentivirus transduction to introduce Cas9 and small guide RNAs (gRNAs) to IP_3R1, IP_3R2, and
119 IP_3R3 (Table 1). The lentivirus construct was designed by our lab and manufactured by
120 VectorBuilder (Chicago, IL). MA104-GCaMP6s cells were transduced with MOI 10 in complete
121 DMEM supplemented with 10 µg/mL polybrene (21). At 72 hours post-transduction, cells were
122 passaged in the presence of 40 µg/mL blasticidin. After 2 weeks of selection, cells were dilution
123 cloned and resulting clones were screened for lack of agonist-induced IP_3R Ca^{2+} responses, as
124 described below.

125 *Sequencing of* IP_3R *triple-knockout*

126 Genomic DNA was extracted using a PureLink™ gDNA mini kit (Invitrogen, USA). PCR
127 amplification was performed using KOD Hotstart polymerase kit (EMD Millipore) and primers
128 flanking the gRNA target sites (Table 2). PCR products were cloned in TOPO-TA vectors

129 (Invitrogen, USA) and a minimum of six bacterial colonies for each IP_3R gene were sequenced
130 using M13 forward and reverse primers (Azenta, NJ, USA). To determine the distribution of
131 mutant alleles, sequences were mapped to the genomic DNA using SnapGene.
132
133 **LLC-MK2-GCaMP6s P2Y1 knock-in generation.**
134 LLC-MK2-GCaMP6s P2Y1 knock in lines were generated by lentiviral transduction of the human
135 P2RY1 receptor. The P2Y1 cDNA clone was purchased from GenScript (Piscataway, NJ, USA),
136 subcloned into pLVX-IRES-Neo (Takara Bio), and packaged by the BCM Vector Development
137 Core. LLC-MK2-GCaMP6s cells were transduced with MOI 10 in 10 μg/mL polybrene and at 72
138 hr post-transduction selected using 500 μg/mL G418. (21). Presence of functional P2Y1 was
139 verified by Ca^{2+} imaging for a Ca^{2+} response to 25 nM ADP.
140
141 **Ca^{2+} agonist treatment.**
142 MA104-GCaMP6s and MA104-GCaMP6s-IP_3R-TKO monolayers were placed in Ca^{2+} free
143 Hank's Balanced Salt Solution (HBSS, Invitrogen) and incubated for ~1 hr to equilibrate. For
144 agonist testing, we used 50 μM ADP for purinergic receptors, 0.75 μM AC55541 or 2 μM
145 Worthington's trypsin for PAR2 receptors, or 1 μM thapsigargin to inhibit SERCA pumps. Cells
146 were first imaged for 30 seconds to establish a baseline. Following agonist stimulation with 50
147 μL of agonist solution, cells were imaged for 2 minutes to capture the peak Ca^{2+} response.
148 Imaging acquisition was 50 ms exposures with a 1 second interval.
149
150 **Live-cell Ca^{2+} imaging of virus infection.**
151 Cell monolayers were grown in Ibidi 8-well chamber slides. On the day of imaging, media was
152 replaced with FluoroBrite-Plus media [FluoroBrite DMEM supplemented with 1X nonessential

153 amino acids, 1X Glutamax, 1X sodium pyruvate, and 15 μM HEPES (Invitrogen)]. Rotavirus was
154 diluted in FluoroBrite-Plus and cells were mock- (FluoroBrite-Plus alone) or rotavirus-infected at
155 MOI 0.01. The inoculum was removed after 1 hr, fresh FluoroBrite-Plus was added, and the slide
156 was mounted into the microscope environmental chamber (37°C in 5% CO_2) to equilibrate.
157 Imaging was performed using a Nikon TiE inverted microscope using a SPECTRAX LED light
158 source (Lumencor) and either a 20x Plan Fluor (NA 0.45) or a 20X Plan Apo (NA 0.75), objective
159 as previously described (20). Nikon Elements Advanced Research v4.5 software was used for
160 data acquisition and image analysis. Fluorescence intensity values were exported to Microsoft
161 Excel and GraphPad Prism for data analyses.
162
163 **Viral infectivity assay.**
164 MA104-GCaMP6s and MA104-GCaMP6s-IP_3R-TKO monolayers grown in 96-well plates were
165 inoculated with 2-fold serial dilutions of SA11-mRuby. The inoculum was removed 1 hr post-
166 infection, then the cells were rinsed twice with PBS and cultured in FBS-free DMEM for ~16 hrs.
167 Monolayers were fixed in ice cold methanol for 20 minutes at 4°C, washed three times with PBS,
168 and immunostained for 2 hrs using a rabbit anti-rotavirus antisera (strain Alabama) at 1:1000 in
169 PBS, followed by incubation for 1 hr with goat anti-rabbit IgG:AlexaFluor555 at 1:1000 in PBS,
170 and quantitation by fluorescence microscopy.
171
172 **Single-cycle and multi-cycle rotavirus yield assay.**
173 MA104-GCaMP6s and MA104-GCaMP6s-IP_3R-TKO monolayers were inoculated with SA11-
174 mRuby for 1 hr. We used an MOI of 0.01 for single-cycle replication assays and 24 PFU/well for
175 multi-cycle replication assays. For single-cycle assays, cells were maintained in DMEM without
176 trypsin, which prevents rotavirus spread due to lack of VP4 spike protein cleavage and harvested
177 at 24 hpi. For multi-cycle assays, cells were maintained in DMEM with 1 µg/mL Worthington's

178 trypsin and harvested at 24-, 48-, 72-, and 96-hpi. Virus titration was performed by plaque assay
179 (see below).
180
181 **Plaque assay.**
182 Monolayers of MA104 or LLC-MK2 cells, or their modified derivatives, were inoculated with 10-
183 fold serial dilutions of virus samples in FBS-free DMEM. After the inoculum was removed, 3 mL
184 of overlay (1.2% Avicel in FBS-free DMEM supplemented with 0.1 mg/mL DEAE dextran and 1
185 μg/mL Worthington's trypsin) was added to each well and plates were incubated for 3-4 days.
186 After removing the overlay, plates were washed and stained with crystal violet or imaged by
187 fluorescence microscopy prior to crystal violet staining.
188
189 **Immunoblot analysis.**
190 Confluent MA104-GCaMP6s and MA104-GCaMP6s-IP_3R-TKO cells inoculated with SA11-
191 mRuby (MOI 10) were harvested in RIPA buffer at 2, 4, 6, 8, and 10 hpi (20). Samples were
192 boiled for 10 minutes at 100°C in SDS-PAGE sample buffer, separated on Tris-glycine 4–20%
193 SDS-PAGE gels (BioRad), and blotted to nitrocellulose, which was blocked with 10% non-fat dry
194 milk in PBS (BLOTTO). Antibodies were diluted in 0.1% BLOTTO and were: rabbit anti-rotavirus
195 [strain Alabama, (1:1000)] (20), rabbit antisera to SA11 NSP4-aa120-146 (1:2000) (24), and
196 mouse anti-GAPDH (1:2000).
197
198 **Immunofluorescence.**
199 MA104 cell monolayers infected with SA11-mRuby (MOI 1) were fixed at 9 hpi, washed, and
200 incubated overnight at 4°C with rabbit antisera against NSP4 (anti-NSP4-aa114-135) and guinea
201 pig antisera against NSP5 (gift from Dr. Mary Estes at Baylor College of Medicine)(24, 25).
202 Monolayers were washed and incubated for 2 hours at room temperature with fluorescent-

203 conjugated secondary antibodies [anti-Rabbit DyLight 488; anti-guinea pig DyLight 549
204 (Rockland)] diluted 1:2000 in PBS. Monolayers were imaged using a 63X objective on a Zeiss
205 LSM980 confocal microscope with Airyscan. Mander's coefficients were determined by
206 calculating the ratio of signal intensity for NSP4 colocalized with that of NSP5 to the overall
207 intensity of the NSP4 signal in a given image following background subtraction. Analyses used
208 three images per group for a total of 46 MA104 parental and 63 MA104-IP_3R-TKO cells.
209

210 **Detection of ADP release from cells.**

211 Confluent MA104-GCaMP6s and MA104-GCaMP6s-IP_3R-TKO cells were infected with SA11-
212 mRuby (MOI 10) and then maintained in 300 µL FluoroBrite-Plus with 20 µM ARL67156, an
213 ecto-ATPase inhibitor. At ~5 hpi, the supernatant was removed and used to treat parental
214 MA104-GCaMP6s cell monolayers to evoke a Ca^{2+} response, which was monitored by live
215 imaging of GCaMP6s fluorescence and quantitated by measuring the maximum increase in
216 GCaMP6s fluorescence after addition of the supernatant. Specificity of the Ca^{2+} response for
217 P2Y1 activation was determined by pretreating cells with 10 µM BPTU, a P2Y1-selective blocker.
218

219 **Quantitative PCR.**

220 LLC-MK2-GCaMP6s and LLC-MK2-GCaMP6s+P2Y1 cells were grown to confluency in a 24-
221 well plate. Total RNA was extracted from cell monolayers using TRIzol (Ambion) according to
222 the manufacturer's instructions. 300 ng of RNA was used to generate cDNA with SensiFAST
223 synthesis reagents (Bioline). Quantitative PCR was performed with Fast SYBR green (Applied
224 Biosystems) with a QuantStudio 3 thermocycler. Purinergic receptor genes were normalized to
225 18s and expression relative to the lowest expressed gene (P2Y12) was calculated using the
226 $\Delta\Delta C_t$ method. Primer sequences have been published previously and can be found in Table 3
227 (26).

228

229 **SA11-mRuby detection in plaques.**

230 Rotavirus SA11-mRuby plaques were visualized by fluorescence microscopy using a Nikon TiE
231 inverted microscope as described above. Images were taken from a 6-well tissue culture plate
232 with a 10X Plan Fluor objective (NA 0.30). Whole-well images were obtained by taking a 15 mm
233 x 15 mm stitch with blending and 10% overlap.

234

235 **Statistical analyses.**

236 Statistics were completed using GraphPad Prism (version 8.4.3). Unless stated, all experiments
237 were performed in biological triplicate. The threshold for Ca^{2+} spikes is a 5% increase in GCaMP
238 fluorescence, as previously defined for this system (20). We performed column statistics to
239 determine the normality of the data sets. We used unpaired Student's t test for data sets with a
240 parametric distribution or a Mann-Whitney test for data sets with a nonparametric distribution.
241 We applied a one-way ANOVA with proper correction when applicable for comparing sample
242 groups to control groups. Differences were determined statistically significant if the P value was
243 <0.05. For all figures, P value notations are as follows: *P <0.05, **P <0.01, ***P <0.001, and
244 ****P <0.0001.

245 **Results**

246 Previous studies have shown that rotavirus NSP4's viroporin function is a critical
247 mechanism for the dysregulation of cellular Ca^{2+} homeostasis during infection (7, 20). Yet, NSP4
248 crosstalk with host IP_3R channels could contribute to the overall Ca^{2+} signaling in infected cells
249 and the recently discovered intercellular Ca^{2+} waves (ICWs) induced by rotavirus are generated
250 by IP_3R Ca^{2+} release upon activation of P2Y1 receptors (14-17). Thus, we investigated the role
251 of IP_3R in the rotavirus-induced Ca^{2+} signaling landscape using IP_3R-null cell lines generated by
252 CRISPR-Cas9 genome editing. First, we obtained IP_3R triple-knockout (IP_3R-TKO) HEK293
253 cells, which express no functional IP_3R isoforms, and tested whether rotavirus infection elevates
254 Ca^{2+} signaling similar to MA104 cells (15). Using long-term, time-lapse Ca^{2+} imaging, we found
255 that rotavirus infected MA104-GCaMP6s cells exhibited increased Ca^{2+} signaling, as we
256 previously described (20). Representative images show both the low amplitude intracellular Ca^{2+}
257 signals observed in rotavirus-infected cells (at 354 min and 360 min), as well as high amplitude
258 ICWs that propagate to surrounding uninfected cells (396 min) (Figure 1A, Movie S1).
259 Representative traces show mock-infected cells exhibit no strong Ca^{2+} signaling events (Figure
260 1B, black line), but rotavirus-infected cells exhibited a strong increase in dynamic Ca^{2+} signaling
261 (Figure 1B, red line). Further, the intracellular Ca^{2+} signals, highlighted in the magenta bracket,
262 occur before the onset of ICWs (Figure 1B). This increase in Ca^{2+} signaling results in significantly
263 more Ca^{2+} spikes in rotavirus-infected than in mock infected cells (Figure 1C).

264 Next, to test the role of IP_3R in dysregulation of Ca^{2+} signaling during rotavirus infection,
265 we examined Ca^{2+} signaling in SA11-mRuby infected parental HEK293-GCaMP6s and HEK293-
266 GCaMP6s-IP_3R-TKO cells (Figure 1D-F). Representative images (Figure 1D) and Ca^{2+} signaling
267 traces (Figure 1E) show that both parental HEK293-GCaMP6s and HEK293-GCaMP6s-IP_3R-
268 TKO cells exhibit robust Ca^{2+} signaling during rotavirus infection (red lines) that is much greater
269 than in mock-infected cells (black lines). We observe numerous intracellular Ca^{2+} signals in both

cell lines but only a few, small ICWs in parental HEK293-GCaMP6s cells. There were no ICWs in the HEK293-GCaMP6s-IP$_3$R-TKO cells because, as a Gq-coupled GPCR, P2Y1 evokes an IP$_3$R-mediated release of ER Ca^{2+} (Figure 1D and Movie S2). Quantitation of Ca^{2+} signaling in parental HEK293-GCaMP6s and HEK-293-GCaMP6s-IP$_3$R-TKO cells show both cell types had a significant increase in overall spikes per cell compared to mock cells (Figure 1F). While we observed a small, but statistically significant, increase in overall Ca^{2+} signaling in HEK293-GCaMP6s-IP$_3$R-TKO cells compared to parental HEK293-GCaMP6s cells (Figure 1F), the critical observation is that there was no *decrease* in rotavirus-induced Ca^{2+} signaling in HEK293-GCaMP6s-IP$_3$R-TKO cells. Together, these data show rotavirus infection produces robust Ca^{2+} signaling in both MA104 and HEK293 cells, and this is not decreased in the absence of IP$_3$R. However, HEK293 cells are suboptimal for examining rotavirus-induced Ca^{2+} signaling, since they do not exhibit robust ICWs and therefore do not have distinct intracellular and intercellular signaling patterns. Thus, for further

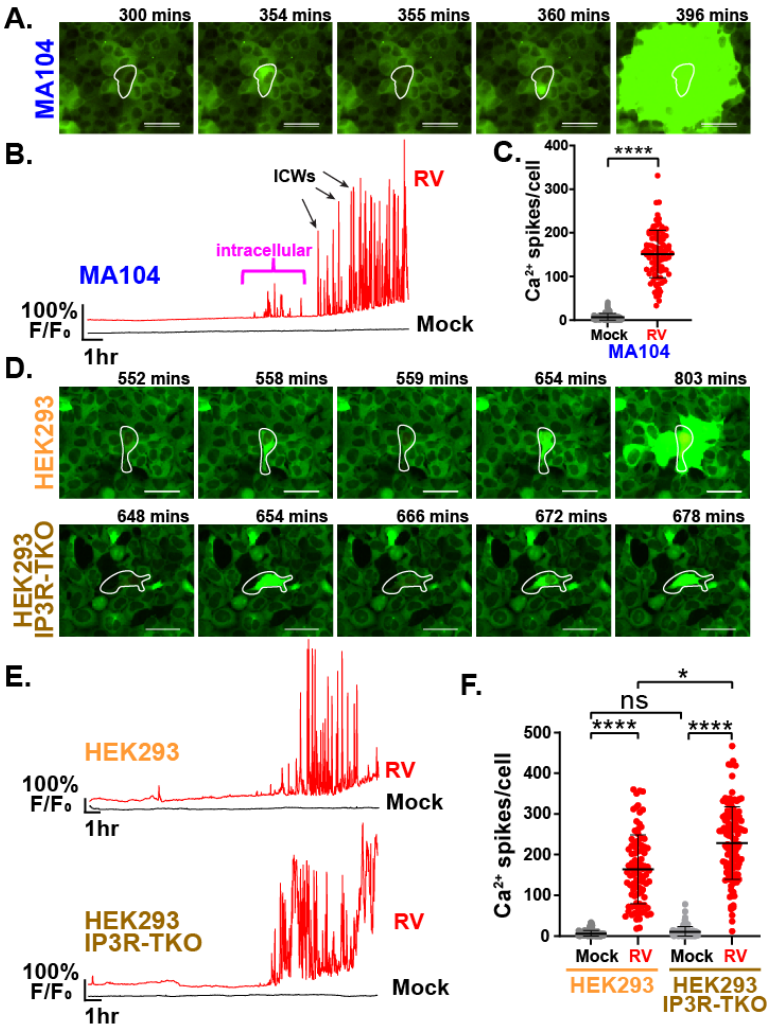

Figure 1. Time lapse Ca^{2+} imaging of rotavirus (RV) infected MA104-GCaMP6s, HEK293-GCaMP6s, and HEK293-GCaMP6s-IP$_3$R-TKO cells. **A.** Filmstrip of a RV infected MA104 cell (white outline) showing both intracellular and intercellular Ca^{2+} signals. **B.** Normalized GCaMP6s fluorescence (F/F_0) of representative mock (black) and RV-infected (red) cells from ~2-20 hpi. Intracellular Ca^{2+} signals (magenta bracket) occurred prior to the onset of ICWs (black arrows = representative ICWs). **C.** Quantitation of Ca^{2+} spikes per cell in mock (grey) or RV-infected (red) cells. ****$p<0.001$ by Mann-Whitney T test. **D.** Filmstrip images of representative HEK293-GCaMP6s and HEK293-GCaMP6s-IP$_3$R-TKO cells (white outline) showing intracellular Ca^{2+} signals over time. **E.** Representative single-cell of normalized GCaMP6s fluorescence from mock (black) and RV-infected (red) HEK293-GCaMP6s and HEK293-GCaMP6s-IP$_3$R-TKO cells. **F.** Quantitation of Ca^{2+} spikes per cell in mock (grey) or RV-infected (red) HEK293-GCaMP6s and HEK293-GCaMP6s-IP$_3$R-TKO cells. Statistical analysis by Kruskal-Wallis with Dunn's multiple correction where *$p<0.05$ and ****$p<0.0001$. All data are displayed as mean ± SD. Scale bars are 50 µm.

295 investigation into the role of IP_3R-mediated signaling during rotavirus infection, we aimed to
296 establish an MA104-GCaMP6s-IP_3R-TKO cell line.

297 **Generation MA104-GCaMP6s cells lacking IP_3R expression.**

298 To generate an MA104-GCaMP6s cell line lacking IP_3R expression, we generated a
299 CRISPR-Cas9 lentivirus construct that expresses individual gRNAs targeted to each IP_3R gene
300 (Table 1). Our workflow to generate MA104-GCaMP6s-IP_3R-TKO cells is depicted in Figure 2A.
301 For screening and validation, we used two different GPCR agonists to activate IP_3R-mediated
302 Ca^{2+} responses: 50 μM ADP to activate P2Y
303 purinergic receptors and 0.75 μM AC55541
304 to activate the Protease-activated Receptor
305 2 (PAR2). We identified 8 clones that
306 exhibited little to no response to these two
307 agonists (Figure 2B) and chose clone F3 for
308 full characterization, which will be designated
309 MA104-GCaMP6s-IP_3R-TKO cells for the
310 remainder of this paper.

311 To functionally validate the loss of
312 IP_3R Ca^{2+} signals in MA104-GCaMP6s-
313 IP_3R-TKO cells, we performed live imaging
314 to measure Ca^{2+} responses to ADP and
315 PAR2 agonist AC55541 (Figure 2C-D). For
316 both agonists, MA104-GCaMP6s-IP_3R-TKO
317 cells exhibit no increase in Ca^{2+} and a small,
318 but reproducible, decrease in GCaMP6s

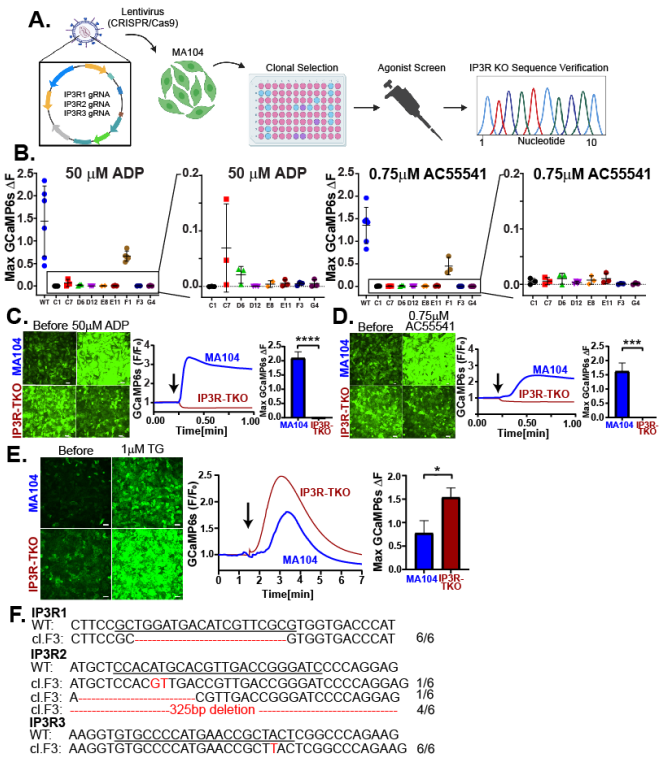

Figure 2. Development of MA104-IP_3R-TKO GCaMP6s cell line. **A.** Schematic workflow for the generation and validation of the MA104-GCaMP6s-IP_3R-TKO cells. **B.** Maximum change in GCaMP6s fluorescence in MA104-GCaMP6s and MA104-GCaMP6s-IP_3R-TKO clones after agonist screening using ADP and AC55541 (PAR2 agonist). **C.** (Left) MA104-GCaMP6s and MA104-GCaMP6s-IP_3R-TKO cells before and after treatment with ADP. Traces (middle) and quantitation (right) of GCaMP6s fluorescence showing Ca^{2+} responses of parental and IP_3R-KO cells upon ADP addition (arrow). **D.** Agonist treatment studies as in (**C**) but using 0.75 μM AC55541. **E.** MA104-GCaMP6s and MA104-GCaMP6s-IP_3R-TKO cells before and after 1 μM thapsigargin treatment. Ca^{2+} signaling traces and quantitation showing normalized GCaMP6s fluorescence after 1 μM thapsigargin treatment (arrow). **F.** Genomic DNA sequencing of IP_3R1, IP_3R2, and IP_3R3 gRNA sites for MA104-GCaMP6s and MA104-GCaMP6s-IP_3R-TKO cells. All data represented as mean ± SD. Statistical analyses were performed by Mann-Whitney test with *p<0.05, ***p<0.001, ****p<0.0001. Scale bars are 50 μm.

319 fluorescence (Figure 2C-D, red traces; Movie S3). To validate these cells, maintain an ER Ca^{2+}
320 store, we treated cells with thapsigargin to inhibit SERCA pumps. We found thapsigargin induced
321 an increase in GCaMP6s fluorescence for both parental and IP_3R-TKO cells, and peak signal
322 from IP_3R-TKO cells was significantly greater than that of parental MA104-GCaMP6s cells
323 (Figure 2E). This indicates that IP_3R-TKO cells have a higher ER Ca^{2+} load than that of parental
324 MA104-GCaMP6s cells, which would be expected in the absence of basal IP_3R activity. Finally,
325 sequence analyses of MA104-GCaMP6s-IP_3R-TKO cells identified the mutations at the gRNA
326 sites for each IP_3R gene. To assess the distribution of mutations, we amplified the gRNA sites
327 for each gene, PCR-cloned amplicons, and sequenced 6 plasmids for each IP_3R gene. We found
328 a deletion mutation for IP_3R1, three different insertion/deletion mutations for IP_3R2 and a single
329 allele insertion for IP_3R3 (Figure 2F), but no wild-type sequences were isolated, consistent with
330 the lack of agonist-induced Ca^{2+} responses from these cells. Together, these data show that we
331 have successfully generated an MA104-GCaMP6s cell line lacking IP_3R expression to better
332 examine the role of IP_3R-mediated ER Ca^{2+} release during rotavirus infection.

333 **Rotavirus-induced Ca^{2+} signaling in the absence of IP_3R.**

334 We previously found that rotavirus infection results in activation of highly dynamic Ca^{2+}
335 signaling throughout infection (20). Now by generating MA104-GCaMP6s-IP_3R-TKO cells, we
336 set out to determine how the lack of IP_3R affects rotavirus-induced Ca^{2+} signaling. We performed
337 long-term, time-lapse Ca^{2+} imaging of both parental MA104-GCaMP6s and MA104-GCaMP6s-
338 IP_3R-TKO cells infected with SA11-mRuby rotavirus, and representative images are shown in
339 Figure 3A. As previously characterized, rotavirus infected parental MA104-GCaMP6s cells
340 exhibit an increase in intracellular Ca^{2+} signals present, as well as production of intercellular
341 Ca^{2+} waves (ICWs) (Figure 3A, top; Movie S4). In MA104-GCaMP6s-IP_3R-TKO cells, we still
342 observed robust intracellular Ca^{2+} signaling in rotavirus-infected cells, but no ICWs were

343 produced (Figure 3A, bottom; Movie S4).
344 Next, we compared Ca^{2+} signaling
345 phenotypes between parental MA104-
346 GCaMP6s and MA104-GCaMP6s-IP_3R-
347 TKO cells, with 4 representative traces for
348 each shown in Figure 3B. We found both
349 cell types exhibit a very similar pattern of
350 robust Ca^{2+} signaling that progressively
351 increases over the course of infection but
352 mock-infected cells exhibited only basal
353 level signaling (Figure 3B). Further, though
354 both cell lines show increased Ca^{2+}
355 signaling dynamics, there were fewer high
356 amplitude Ca^{2+} signals in MA104-
357 GCaMP6s-IP_3R-TKO cells, which likely
358 represents autocrine activation of P2Y1

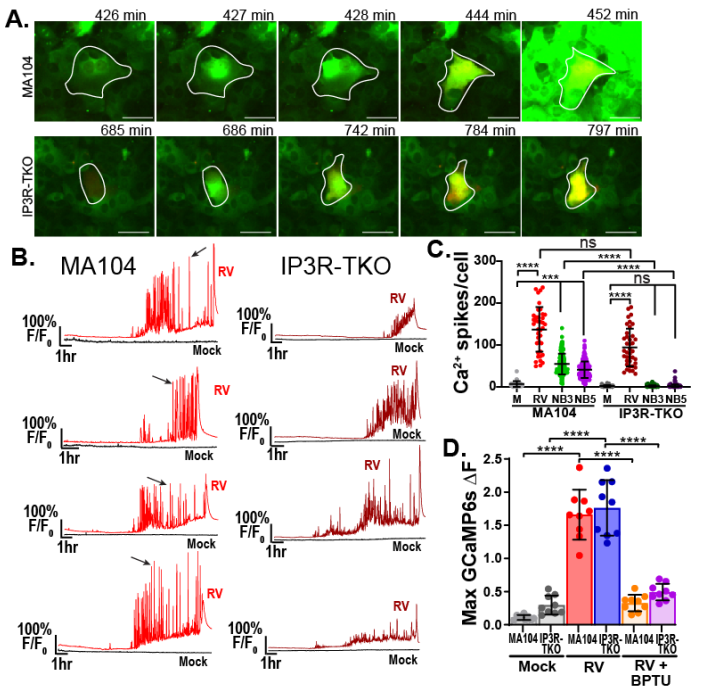

Figure 3. Characterization of MA104-GCaMP6s and MA104-GCaMP6s-IP_3R-TKO cells (IP_3R-TKO) during RV infection. **A.** Filmstrip images of RV infected MA104-GCaMP6s cells (white outline, top row) and MA104-GCaMP6s-IP_3R-TKO cells (white outline, bottom row) overtime. **B.** Four representative single-cell traces of normalized GCaMP6s fluorescence (F/F_0) from mock (black) or RV-infected MA104-GCaMP6s cells (red) or MA104-GCaMP6s-IP_3R-TKO cells (maroon) Arrows indicate example occurrences of an intercellular Ca^{2+} wave signal. **C.** Quantitation of the number of Ca^{2+} spikes per cell in mock (grey), RV-infected and neighboring cells for MA104-GCaMP6s and MA104-GCaMP6s-IP_3R-TKO cells. **D.** Maximum change in normalized GCaMP6s fluorescence after supernatant transfer of RV infected MA104-GCaMP6s (red) and MA104-GCaMP6s-IP_3R-TKO (blue) cells to MA104-GCaMP6s sensor cells treated with 10μM BPTU. All data are shown as the mean ± SD. Statistical analyses were performed using Kruskal-Wallis with Dunn's multiple corrections tests with ***p<0.001 & ****p<0.0001. Scale bars are 50 μm.

359 during ICWs (Figure 3B, arrows). Next, we quantitated the number of Ca^{2+} spikes in rotavirus-
360 infected and uninfected neighboring cells 3 and 5 cells away (NB3 and NB5, respectively) to
361 capture ICWs (Figure 3C). In parental MA104-GCaMP6s cells, we found a significant increase
362 in Ca^{2+} signaling in both infected and neighboring cells, consistent with our previous studies (20).
363 In MA104-GCaMP6s-IP_3R-TKO cells, there was a significant increase in Ca^{2+} signaling in
364 rotavirus-infected cells but no increase in the neighboring cells, consistent with the lack of ICWs
365 (Figure 3C). Interestingly, in rotavirus-infected MA104-GCaMP6s-IP_3R-TKO cells, we found no
366 significant decrease in overall Ca^{2+} signaling (Figure 3C). Since MA104-GCaMP6s-IP_3R-TKO
367 cells did not produce ICWs, we wanted to determine whether the cells were still releasing ADP

368 during infection. To test this, parental MA104-GCaMP6s and MA104-GCaMP6s-IP_3R-TKO cells
369 were mock or rotavirus-infected and incubated in the presence of ARL67156, an ecto-
370 nucleotidase inhibitor, to stabilize extracellular purines. At 5 hpi, a time point when ICWs have
371 begun, media was removed from mock and infected cells and added to parental MA104-
372 GCaMP6s cells. We found that media from rotavirus-infected cells induced a significantly greater
373 Ca^{2+} response than that from mock infected cells, and the Ca^{2+} response was blocked by the
374 P2Y1 inhibitor BPTU (Figure 3D). Together, this indicated that the loss of IP_3R does not reduce
375 the rotavirus-induced release of ADP during infection and that the IP_3R-independent arms of the
376 P2Y1 signaling pathway are likely intact. These data in MA104 cells echo that of our initial
377 studies in HEK293-GCaMP6s-IP_3R-TKO cells, in that rotavirus still dramatically increases Ca^{2+}
378 signaling within infected cells in the absence of IP_3R (Figure 1E). Yet, loss of IP_3R resulted in
379 the abrogation of rotavirus induced ICWs and significantly reduced the increase in Ca^{2+} signaling
380 in surrounding uninfected cells, which ultimately changes the overall Ca^{2+} signaling landscape
381 during infection.

382

383 **Role of IP_3R in rotavirus infection and replication.**

384 Numerous studies have confirmed that increased cytosolic Ca^{2+} is critical for rotavirus
385 replication (12, 13, 27). Thus, we next used parental MA104-GCaMP6s and MA104-GCaMP6s-
386 IP_3R-TKO cells to assess whether IP_3R signaling plays a role in rotavirus infectivity and/or
387 replication. First, we compared SA11-mRuby plaque phenotypes between parental MA104-
388 GCaMP6s and MA104-GCaMP6s-IP_3R-TKO cells, discovering a major difference in plaque
389 morphology (Figure 4A). MA104-GCaMP6s cell plaques fully cleared the monolayer and had
390 clean margins (Figure 4A, Top) in contrast to MA104-GCaMP6s-IP_3R-TKO cells, which exhibited
391 a similar number of plaques (i.e., no difference in measured titer); however, the plaques were

turbid with most of the monolayer remaining intact (Figure 4A, Bottom). Quantification of plaque diameters showed rotavirus formed significantly smaller plaques on MA104-GCaMP6s-IP$_3$R-TKO cells than on parental MA104-GCaMP6s cells (Figure 4A). Due to this substantial difference in plaque formation, we next determined whether loss of IP$_3$R affected rotavirus infectivity or single-cycle virus yield. We first determined infectivity of SA11-mRuby for both parental MA104-GCaMP6s and MA104-GCaMP6s-IP$_3$R-TKO cells using a fluorescent focus assay (FFA) and found no differences in the observed titer, indicating that rotavirus infects both cell lines with the same efficiency (Figure 4B). This is consistent with both our live imaging studies (Figure 3) and plaque assays (Figure 4A), in which we observed a similar number of infected cells and plaques, respectively. Next, we tested whether the MA104-GCaMP6s-IP$_3$R-TKO cells efficiently supported rotavirus replication. We compared single-cycle virus yield between parental MA104-GCaMP6s and MA104-GCaMP6s-IP$_3$R-TKO cells. Cells were infected with MOI 0.01 and maintained in the absence of trypsin to limit the infection to a single round. We found that yields were similar between parental MA104-GCaMP6s and MA104-

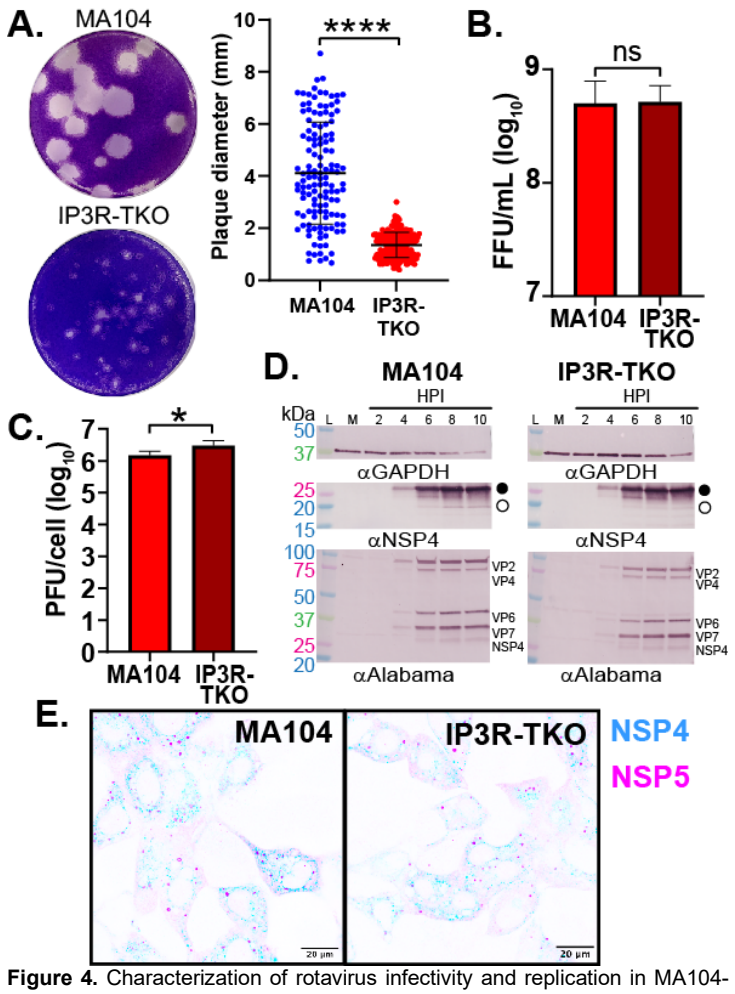

Figure 4. Characterization of rotavirus infectivity and replication in MA104-GCaMP6s-IP$_3$R-TKO cells. **A.** Representative images and diameter quantitation of RV plaques formed on MA104-GCaMP6s or MA104-GCaMP6s-IP$_3$R-TKO cells. **B.** Quantitation of rotavirus infectivity by FFA on MA104-GCaMP6s (red) or MA104-GCaMP6s-IP$_3$R-TKO (dark red) cells. **C.** One-step rotavirus yield from MA104-GCaMP6s (red) or MA104-GCaMP6s-IP$_3$R-TKO (dark red) cells was measured by plaque assay and graphed as Log$_{10}$ plaque forming units (PFU) per cell. **D.** Kinetics of rotavirus protein expression in MA104-GCaMP6s and MA104-GCaMP6s-IP$_3$R-TKO cells was determined by immunoblot for GAPDH (top), NSP4 (middle), and a rabbit anti-rotavirus (strain Alabama) (bottom). **E.** Immunofluorescence of RV-infected MA104-GCaMP6s and MA104-GCaMP6s-IP$_3$R-TKO cells to detect NSP4 (blue) and NSP5 (magenta), as a marker of viroplasms. All data are shown as the mean ± SD. Statistical analyses were performed using Mann-Whitney T tests with *$p<0.05$ & ****$p<0.0001$. Scale bars are 20 µm.

417 GCaMP6s-IP_3R-TKO cells, though there was a small increase in rotavirus yield in MA104-
418 GCaMP6s-IP_3R-TKO cells (Figure 4C). Thus, the small plaque phenotype on the MA104-
419 GCaMP6s-IP_3R-TKO cells cannot be explained by an inability of these cells to support rotavirus
420 replication. We evaluated rotavirus protein expression by western blot and found similar levels
421 and kinetics of viral protein synthesis for both structural proteins and NSP4 in both cell lines
422 (Figure 4D). Finally, we using immunofluorescence staining of rotavirus-infected cells, we found
423 no difference in viroplasm formation localization of NSP4 to viroplasms (Figure 4E) and this was
424 confirmed by determining no significant difference in the Manders' coefficient for each cell
425 (MA104: 0.047±0.018; MA104-IP_3R-TKO: 0.034±0.013, $p=0.7$). Together, these data indicate
426 the loss of IP_3R did not significantly affect the ability of rotavirus to infect, produce proteins, or
427 assemble new progeny virus during the initial round of replication, and therefore suggests the
428 defect in plaque formation occurs during rotavirus spread through multiple rounds of replication.
429

430 **Role of IP_3R and ICWs in rotavirus spread.**

431 To further investigate why rotavirus did not plaque efficiently on MA104-GCaMP6s-IP_3R-
432 TKO cells, we used fluorescent microscopy to examine the spread of SA11-mRuby in the area
433 around plaques for both parental MA104-GCaMP6s and MA104-GCaMP6s-IP_3R-TKO cells. We
434 performed plaque assays with SA11-mRuby and, on day 4 post-infection, we replaced the
435 overlay with PBS and imaged plaques by brightfield and fluorescence microscopy to visualize
436 mRuby expression in the plaques. In parental MA104 cells, there was full clearing of the plaque
437 and strong mRuby expression in a wide margin around the plaque (Figure 5A, top). In contrast,
438 plaques on MA104-GCaMP6s-IP_3R-TKO cells do not clear and the area of mRuby-positive cells
439 were substantially smaller (Figure 5A, bottom).

440 Next, we examined whether the smaller, turbid plaques formed on MA104-GCaMP6s-
441 IP_3R-TKO cells were the result of a decrease in virus replication kinetics in multi-step replication.

We infected parental MA104-GCaMP6s and MA104-GCaMP6s-IP_3R-TKO cells with ~24 PFU (MOI = ~5.9×10^{-5}) to ensure well isolated infected cells, and cultured in the presence of trypsin to visualize SA11-mRuby spread and measure the kinetics of virus replication over 96-hours post-infection. Using live microscopy, we tracked SA11-mRuby spread throughout the monolayer in both parental MA104-GCaMP6s and MA104-GCaMP6s-IP_3R-TKO cells (Figure 5B). In parental MA104-GCaMP6s cells, there was more rapid spread with complete destruction of the monolayer by 48-72 hpi (Figure 5B, top). In contrast, virus spread in MA104-GCaMP6s-IP_3R-TKO cells was substantially delayed, especially between 24-48 hpi (Figure 5B, bottom). Next, we determined virus yield from 24-96 hpi and found parental MA104-GCaMP6s cells supported faster virus replication than MA104-GCaMP6s-IP_3R-TKO cells, with peak titers reached in parental cells by 48 hpi (Figure 5C, red line). In contrast, virus replication was significantly lower in MA104-GCaMP6s-IP_3R-TKO cells from 48-72 hpi and did not peak until 72-96 hpi (Figure 5C, blue line).

Finally, we examined rotavirus spread using live, time-lapse microscopy to measure the rate of mRuby expression in the absence or presence of trypsin (Figure 5D). As was shown in Figure 3A, in the absence of trypsin there are single infected cells and no spread of mRuby to neighboring cells (data not shown). In the presence of trypsin, rotavirus spread

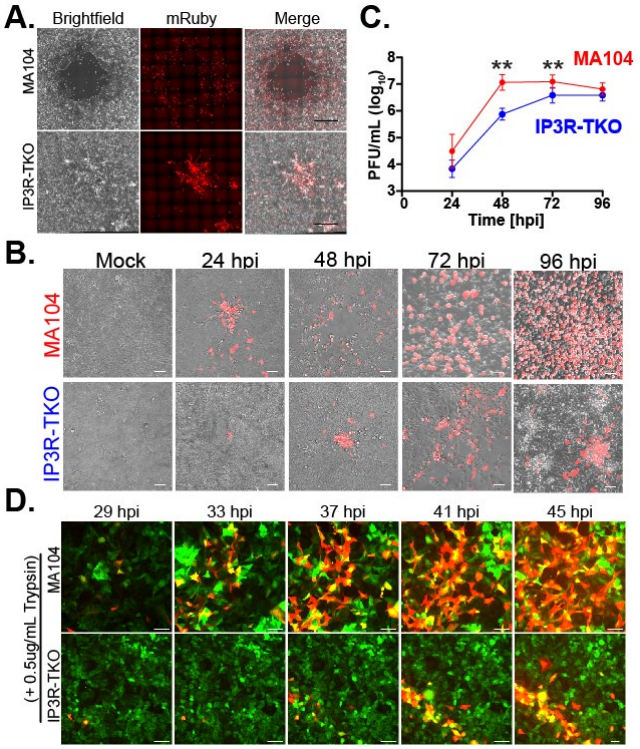

Figure 5. Loss of IP_3R reduces rotavirus spread. **A.** Visualization of SA11-mRuby in plaques from MA104-GCaMP6s or MA104-GCaMP6s-IP_3R-TKO cells. Brightfield (left) and SA11-mRuby fluorescence (middle) images are merged on the right. Images were acquired with a Plan Fluor objective (NA 0.30) with 10x10mm stich parameters. Scale bars are 1000 µm **B.** SA11-mRuby spread in MA104-GCaMP6s (red) or MA104-GCaMP6s-IP_3R-TKO (blue) cells. Brightfield and fluorescence (SA11-mRuby) images were acquired at the indicated times post infection using a 20x Plan Fluor objective (NA 0.45). **C.** SA11-mRuby yield from 24-96 hpi from MA104-GCaMP6s (red) or MA104-GCaMP6s-IP_3R-TKO cells (blue) was measured by plaque assay and graphed as Log_{10} PFU/mL. **D.** Live imaging of SA11-mRuby (RFP) spread in GCaMP6s-expressing parental MA104-GCaMP6s (top) or MA104-GCaMP6s-IP_3R-TKO cells (bottom) from ~30-45 hpi. All data are shown as the mean ± SD. Scale bars are 50 µm in B & D. **$p<0.01$ by T-test.

466 rapidly from the initial infected cells to many of the surrounding cells in parental MA104-
467 GCaMP6s cells, but in MA104-GCaMP6s-IP_3R-TKO cells, this was much slower and primarily
468 to adjacent cells (Figure 5D, Movie S5). Together, these data show that in infected cells, the
469 host IP_3R ER Ca^{2+} channel is largely for dispensable rotavirus-induced in Ca^{2+} signaling;
470 however, IP_3R-mediated Ca^{2+} signaling was critical for rotavirus replication and spread.

471

472 **Priming Uninfected Cells via P2Y1-mediated ICWs.**

473 As the loss of IP_3R did not affect rotavirus infectivity or replication in the single cycle
474 replication studies, the above data indicated the defect in rotavirus spread was related to the
475 lack of increased Ca^{2+} signaling in neighboring cells.
476 Increased Ca^{2+} signaling in rotavirus-infected cells has
477 been shown to be critical for robust replication (12, 28,
478 29), so these observations led us to hypothesize that
479 the increased Ca^{2+} signaling in neighboring uninfected
480 cells could promote rotavirus replication/spread by
481 priming them for infection. Thus, we set out to test this
482 hypothesis by examining how the manipulation of ICWs
483 affected rotavirus spread.

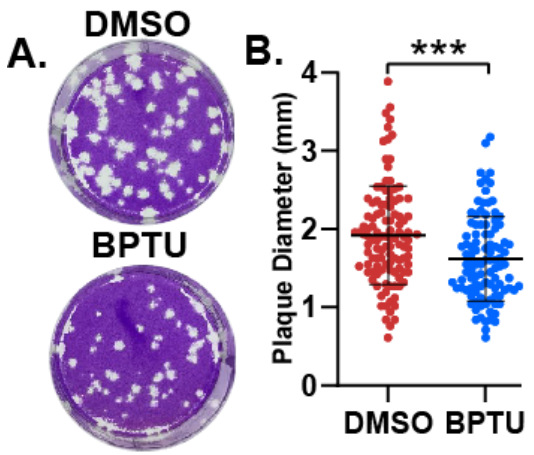

Figure 6. Blocking P2Y1-mediated ICWs reduces rotavirus plaque size. **A.** Representative image of RV plaques formed on parental MA104 cell monolayers treated with DMSO (Top) or 1 μM BPTU (bottom). **B.** Measurement of plaque diameter for DMSO and 1 μM BPTU treated cells. Data are shown as the mean ± SD. ***p<0.001 by Mann-Whitney T test.

484 We previously showed P2Y1 receptor blockers significantly inhibits rotavirus induced
485 ICWs (17). Thus, we next tested whether blocking ICWs with BPTU, a P2Y1 selective blocker,
486 would also reduce rotavirus spread. We performed a plaque assay using parental MA104 cells
487 in the presence of 1 μM BPTU, or DMSO vehicle control, and found BPTU treatment resulted in
488 significantly smaller plaques (Figure 6). Thus, reducing ICWs by blocking P2Y1 causes a similar
489 reduction in the ability of rotavirus to form plaques as the loss of IP_3R; however, P2Y1 blockers,

or even P2Y1 knockout cells, did not fully abrogate ICWs as strongly as MA104-GCaMP6s-IP$_3$R-TKO cells (17). Therefore, to further test the role of ICWs in rotavirus replication, we examined rotavirus spread in LLC-MK2-GCaMP6s cells, a rhesus monkey kidney cell line we used previously to study Ca^{2+} signaling by Recoviruses (Rhesus enteric caliciviruses) (22). We observed that while rotavirus-infected LLC-MK2-GCaMP6s cells exhibited increased Ca^{2+} signaling, there were no ICWs and therefore no increase in Ca^{2+} signaling in neighboring uninfected cells (Figure 7A). Further, treatment of LLC-MK2-GCaMP6s cells with ADP did not evoke a Ca^{2+} response (Figure 7B, D), indicating a lack of functional P2Y1 signaling. So, we reasoned that if ICWs are a critical factor in rotavirus spread, exogenous expression of P2Y1 in LLC-MK2-GCaMP6s cells might rescue the rotavirus-induced ICW phenotype and increased rotavirus spread. We used lentivirus transduction to generate a stable P2Y1 knock-in LLC-MK2-GCaMP6s cell line (LLC-MK2-GCaMP6s+P2Y1) and presence of an ADP-stimulated Ca^{2+} signal confirmed the P2Y1 was functional in these cells (Figure 7C-D, Movie S6). We confirmed a significant increase in P2Y1 expression in the LLC-MK2-GCaMP6s+P2Y1 cells by qRT-PCR and found that the P2Y1 knock-in did not affect the expression of any other P2Y purinergic receptor (Figure 7E).

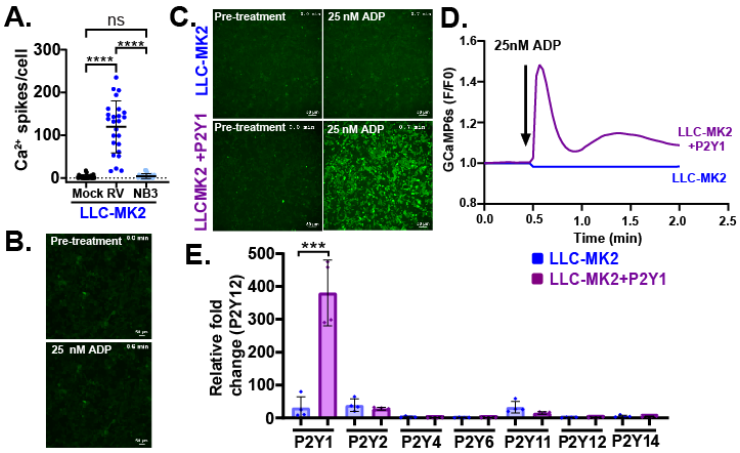

Figure 7. P2Y1 Ca^{2+} signaling in LLC-MK2 cells. **A.** Ca^{2+} spikes per cell in mock (black), rotavirus-infected (blue), and neighboring (NB3) uninfected (light blue) cells. ****p<0.0001 by Kruskal-Wallis with Dunn's multiple corrections. **B.** Representative images of LLC-MK2 cell monolayers before (top) and after (bottom) treatment with 25 nM ADP. **C.** Representative images of LLC-MK2 and LLC-MK2+P2Y1 cell monolayers before (left) or after (right) agonist treatment with 25nM ADP. **D.** Ca^{2+} signaling traces of LLC-MK2 (blue line) and LLC-MK2+P2Y1 cells (purple line) after treatment with 25 nM ADP (arrow). **E.** P2Y purinergic receptor mRNA expression by qPCR in LLC-MK2 and LLC-MK2+P2Y1 cells. Data were normalized to 18s mRNA and plotted relative to P2Y12 mRNA transcript levels. ***p<0.0001 by individual T tests. All data represented as mean ± SD. Scale bars are all 50 µm.

We next investigated whether exogenous expression of P2Y1 was able to rescue the rotavirus-induced ICWs and, if this affected rotavirus spread. We performed live imaging of

514 rotavirus-infected LLC-MK2-GCaMP6s+P2Y1 cells and found these cells exhibited both higher
515 basal Ca^{2+} signaling and ICWs that originate from rotavirus-infected cells (Figure 8A, Movie S7),
516 resulting in greater Ca^{2+} signaling in the neighboring, uninfected cells than mock-inoculated cells
517 (Figure 8B). Next, we used plaque assays to assess rotavirus spread in LLC-MK2-GCaMP6s
518 cells. In parental LLC-MK2-GCaMP6s cells, rotavirus formed few plaques and those visible were
519 turbid (Figure 8C, top); however, LLC-MK2-GCaMP6s+P2Y1 cells showed more plaques with
520 greater clearing (Figure 8C, bottom). We used fluorescent microscopy to examine spread of
521 SA11-mRuby in the area around plaques for
522 both cell lines. We saw strong mRuby
523 expression for both cell types, but LLC-
524 MK2-GCaMP6s+P2Y1 had significantly
525 more infected cells surrounding the plaques
526 regions with cell monolayer clearing (Figure
527 8D-E). Thus, introducing P2Y1 expression
528 in LLC-MK2-GCaMP6s cells provides a
529 gain-of-function to produce ICWs in
530 response to rotavirus-infection and this
531 results in better plaque formation and more
532 efficient virus spread. Together these data
533 support our model that the Ca^{2+} signals from
534 P2Y1-mediated ICWs, which requires ER
535 Ca^{2+} release by IP_3R, and primes
536 neighboring cells to promote more robust
537 rotavirus replication and spread *in vitro*.

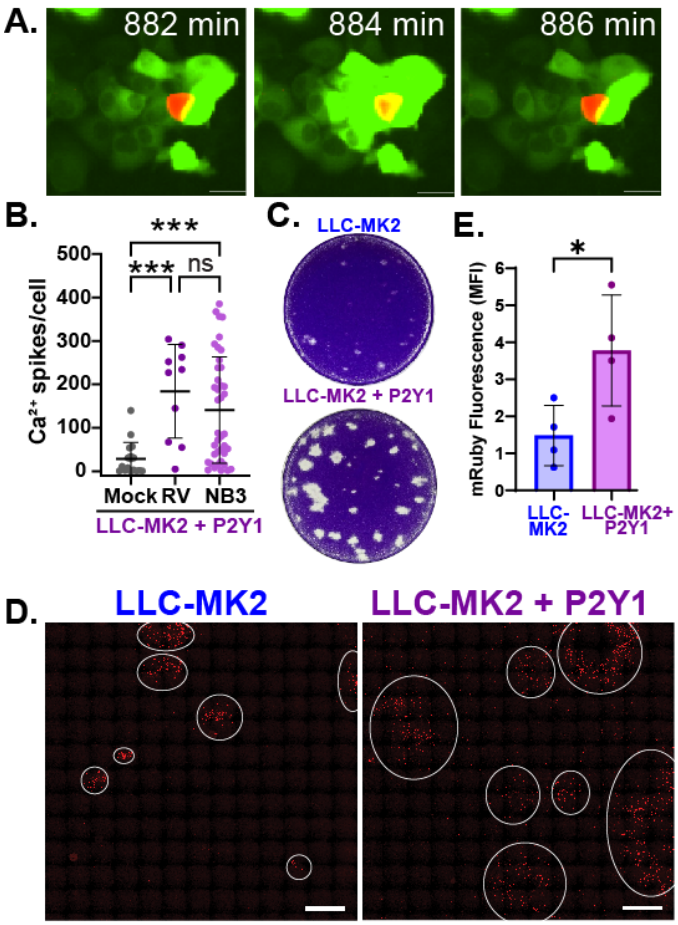

Figure 8. Reconstituting ICWs in LLC-MK2+P2Y1 cells increases rotavirus spread. **A.** Filmstrip images of RV ICWs in LLC-MK2+P2Y1 cells. Scale bar is 50 µm. **B.** Ca^{2+} spikes per cell in mock or RV infected and neighboring (NB3) LLC-MK2 cells. ***$p<0.001$ by Kruskal-Wallis with Dunn's multiple correction test. **C.** Representative images of RV plaques formed on LLC-MK2 (Top) and LLC-MK2+P2Y1 (bottom) monolayers. **D.** RV infected (red) LLC-MK2 (left) and LLC-MK2+P2Y1 (right) cell monolayers. White circles designate the margins of RV foci. Images were captured using a Plan Fluor 10x objective (NA 0.30) with 15 x15 mm stich parameters. In these stitched images, the scale bar represents 2000 µm. **E.** Quantitation of mean fluorescence intensity of TRITC channel. *$p<0.05$ by Mann-Whitney T-test. All data are shown as the mean ± SD.

538 **Discussion**

539 A hallmark of rotavirus infection, and several other viruses, is an elevation in cytosolic
540 Ca^{2+} and decrease in ER Ca^{2+} stores, which facilitates virus replication and contributes to
541 pathogenesis through a variety of downstream pathways. Host cells also rely on Ca^{2+} signaling
542 pathways to maintain homeostasis. The IP_3R Ca^{2+} channel is an important Ca^{2+} signaling relay
543 hub converting extracellular signals (e.g., ADP) into intracellular signals in which Ca^{2+} itself is
544 the second messenger that controls a myriad of cellular pathways via Ca^{2+}-regulated proteins
545 (30). While the NSP4 viroporin initiates the dysregulation of Ca^{2+} homeostasis during rotavirus
546 infection, the role of IP_3R in generating rotavirus-induced Ca^{2+} signals, particularly in virus-
547 infected cells, had not been characterized. By developing a MA104-GCaMP6s-IP_3R-TKO cell
548 line, we uncovered the following: (i) IP_3R is not required for elevated Ca^{2+} signaling observed in
549 rotavirus-infected cells; (ii) IP_3R ER Ca^{2+} release is critical for P2Y1-mediated ICWs that
550 increase Ca^{2+} signaling in neighboring, uninfected cells; and (iii) while IP_3R Ca^{2+} signaling is not
551 *necessary* for rotavirus replication, the rotavirus-induced ICWs, which require IP_3R, increase the
552 kinetics of rotavirus replication and spread *in vitro*. Together, these findings indicate that
553 increased Ca^{2+} signals in neighboring cells, caused by ICWs, primes these cells to better support
554 rotavirus replication. This process of 'pre-emptively priming' uninfected cells within a viral niche
555 represents a novel mechanistic paradigm by which viruses exploit intercellular host responses
556 to promote their replication.

557 We recently showed that rotavirus-induced increases in cytosolic Ca^{2+} occur through a
558 massive increase in discrete Ca^{2+} signaling events, and a substantial part of this signaling comes
559 from the release of ER Ca^{2+} (20). By examining IP_3R-null cells (both HEK293 and MA104), we
560 have been able to differentiate two distinct types of Ca^{2+} signals that are induced during rotavirus
561 infection: (1) the intracellular Ca^{2+} signals that occur within rotavirus-infected cells, which were
562 IP_3R-independent, and (2) the multicellular ICWs that propagate from infected to neighboring,

563 uninfected cells, which are IP_3R-dependent. By dissecting out these distinct Ca^{2+} signals, we
564 can gain new mechanistic insights into how these signals support rotavirus replication and
565 spread.

566 The intracellular Ca^{2+} signals are IP_3R-independent, as knockout of IP_3R did not reduce
567 the number of Ca^{2+} signals observed. Since NSP4 alone is sufficient to increase Ca^{2+} signaling
568 by release of ER Ca^{2+}, we propose that the Ca^{2+} signals observed in the IP_3R-TKO cells are ER
569 Ca^{2+} release events by the NSP4 viroporin (27, 31); however, some of these Ca^{2+} signals could
570 be Ca^{2+} entry via SOCE channels (e.g., Orai) activated by NSP4-mediated decrease in ER Ca^{2+}
571 levels (28). The elevation in Ca^{2+} signaling, in the absence of IP_3R, was sufficient to support
572 rotavirus replication, though the kinetics of multi-step virus replication was impaired (discussed
573 below). The fact that rotavirus encodes an intrinsic capability to drive this degree of Ca^{2+}
574 dysregulation further highlights the critical role Ca^{2+} signaling by NSP4, and perhaps other
575 viroporins, plays in virus replication (3, 7, 12). This raises the question of what cellular pathways
576 are activated by these intracellular Ca^{2+} signals. NSP4 viroporin Ca^{2+} signals are critical for
577 rotavirus replication by initiating the cellular autophagy pathway via activation of the Ca^{2+}-
578 dependent kinase CaMKKβ (12). Further, these dynamic ER Ca^{2+} signals increase mitochondrial
579 metabolism and suppress the activation of apoptosis, which would also benefit rotavirus
580 replication (20). Yet, unraveling the complexity of virus-induced Ca^{2+} signaling remains a
581 burgeoning field, so we are certainly to discover other Ca^{2+}-regulated pathways involved in virus
582 replication.

583 While IP_3R Ca^{2+} signaling was dispensable for rotavirus replication, MA104-GCaMP6s-
584 IP_3R-TKO cells revealed rotavirus induced ICWs significantly increased rotavirus spread and the
585 rate of virus replication. The importance of this paracrine ADP/P2Y1-generated ICW signaling
586 pathway was further supported by rescue of rotavirus plaque formation and increased spread in

587 LLC-MK2-GCaMP6s cells when rotavirus ICW generation was reconstituted by exogenous
588 P2Y1. Further, because MA104-GCaMP6s-IP_3R-TKO cells still released ADP, we can infer that
589 the loss of IP_3R Ca^{2+} signaling, and not other downstream effects of P2Y1 activation, cause the
590 defect in rotavirus spread. Since MA104-GCaMP6s-IP_3R-TKO cells supported replication similar
591 to parental MA104-GCaMP6s cells, these data indicate that IP_3R increased rotavirus replication
592 and spread via an increase in Ca^{2+} signaling in neighboring, uninfected cells through the P2Y1-
593 mediated ICWs.

594 Based on these data, we propose the rotavirus-induced ICWs activate pro-viral Ca^{2+}-
595 regulated pathways in neighboring cells, ultimately priming these cells for more rapid and/or
596 increased replication. This raises the question of which Ca^{2+}-regulated pathways are activated
597 by ICWs in neighboring cells and how do they increase rotavirus replication. One likely pathway
598 is the activation of autophagy because ICWs, like NSP4-mediated Ca^{2+} signals, are generated
599 by release of ER Ca^{2+} and IP_3R Ca^{2+} release can activate CaMKKβ and AMPK phosphorylation
600 and upregulate autophagy (32-34). In rotavirus-infected cells, early autophagosome membranes
601 are usurped to traffic NSP4 and VP7 out of the ER and form a membrane compartment
602 associated with viroplasms (i.e., virus replication complexes) which is the site of final rotavirus
603 assembly (12). Thus, ICWs could activate the early, biosynthetic stages of the autophagy
604 pathway, making more of these membranes available to be utilized upon rotavirus infection.

605 Rotavirus-induced Ca^{2+} signaling is also associated with a broad dysregulation in the
606 actin cytoskeleton, though this has primarily been studied in infected or NSP4 expressing cells
607 and the potential role for ICWs has not been investigated (35). Nevertheless, ICWs are an
608 important mode of multicellular epithelial signaling that directs cell extrusion from monolayers in
609 response to cell damage (36-38). The resulting IP_3R-mediated ER Ca^{2+} release triggers a global,
610 but transient, actin reorganization process termed Ca^{2+}-mediated Actin Reset (CaAR) (39). The

611 CaAR response can drive significant changes in host gene transcription by releasing
612 transcription factors otherwise sequestered in the cytosol (39), and this may help identify cellular
613 pathways activated by ICWs. Importantly, the CaAR responses studied thus far have come from
614 singular signals/damage events, but during rotavirus infection, neighboring cells are stimulated
615 by hours of ICWs, providing ample time and numbers of signals to drive substantial changes.
616 Thus, it will likely require a detailed, multi-omics approach to identify ICW-response pathways
617 and elucidate which of those support rotavirus spread.

618 In summary, we have uncovered a dichotomous role for IP_3R in the overall Ca^{2+} signaling
619 landscape during rotavirus infection and in rotavirus replication and spread. Within infected cells,
620 rotavirus (presumedly via NSP4) generates sufficient Ca^{2+} signaling to support its replication
621 without IP_3R, making this host channel dispensable. In contrast, rotavirus spread was increased
622 by the presence of ICWs and therefore increased Ca^{2+} signaling in neighboring cells, essentially
623 priming them for future rotavirus infection. This implies that viral take-over of the infection niche
624 goes beyond rotavirus-infected cells to include nearby uninfected cells, which undergo
625 "preemptive reprogramming" by repeated ICWs prior to becoming infected. Further, ICWs
626 triggered by rotavirus infection may be a common host response to many different virus
627 infections, and, if so, this P2Y1-mediated Ca^{2+} signaling pathway would have a broader
628 importance in virus replication and pathogenesis. Finally, purinergic signaling is just one of the
629 myriad of other intercellular signaling molecules/pathways that could be exploited by viruses to
630 prime or otherwise reprogram uninfected cells within the infection niche. Identification of
631 analogous virus-induced intercellular signaling pathways may uncover new mechanisms by
632 which viruses, or other microbes, exploit host responses to benefit their replication and spread.

633

Acknowledgments.

We thank Dr. David I. Yule at University of Rochester Medical School for his expertise and advise in generating and characterizing the MA104-GCaMP6s-IP_3R-TKO cells. This work was supported in part by NIH grants R01DK115507 and R01AI158683 (PI: J. M. Hyser). Trainee support for J.L.P. was provided by NIH grants F31AI169983 (PI: J. L. Perry). Trainee support for F.J.S. was provided by NIH grants F31DK132942 (PI: F. J. Scribano). Trainee support for J.T.G was provided by NIH grants F30DK131828 and Histochemical Society Graduate Medical Trainee and Graduate Student Cornerstone Grant (PI: J.T. Gebert). Trainee support for K.A.E. was provided by NIH grants F32DK130288 and Histochemical Society Postdoctoral Keystone Grant. Lentivirus packaging of the P2Y1 expression construct was supported by the ATC Gene Vector Core at Baylor College of Medicine.

645 **Figure Legends.**

646 **Figure 1.** Time lapse Ca^{2+} imaging of rotavirus (RV) infected MA104-GCaMP6s, HEK293-
647 GCaMP6s, and HEK293-GCaMP6s-IP_3R-TKO cells. **A.** Filmstrip of a RV infected MA104 cell
648 (white outline) showing both intracellular and intercellular Ca^{2+} signals. **B.** Normalized GCaMP6s
649 fluorescence (F/F_0) of representative mock (black) and RV-infected (red) cells from ~2-20 hpi.
650 Intracellular Ca^{2+} signals (magenta bracket) occurred prior to the onset of ICWs (black arrows =
651 representative ICWs). **C.** Quantitation of Ca^{2+} spikes per cell in mock (grey) or RV-infected (red)
652 cells. ****$p<0.001$ by Mann-Whitney T test. **D.** Filmstrip images of representative HEK293-
653 GCaMP6s and HEK293-GCaMP6s-IP_3R-TKO cells (white outline) showing intracellular Ca^{2+}
654 signals over time. **E.** Representative single-cell of normalized GCaMP6s fluorescence from
655 mock (black) and RV-infected (red) HEK293-GCaMP6s and HEK293-GCaMP6s-IP_3R-TKO
656 cells. **F.** Quantitation of Ca^{2+} spikes per cell in mock (grey) or RV-infected (red) HEK293-
657 GCaMP6s and HEK293-GCaMP6s-IP_3R-TKO cells. Statistical analysis by Kruskal-Wallis with
658 Dunn's multiple correction where *$p<0.05$ and ****$p<0.0001$. All data are displayed as mean ±
659 SD. Scale bars are 50 μm.

660

661 **Figure 2.** Development of MA104-IP_3R-TKO GCaMP6s cell line. **A.** Schematic workflow for the
662 generation and validation of the MA104-GCaMP6s-IP_3R-TKO cells. **B.** Maximum change in
663 GCaMP6s fluorescence in MA104-GCaMP6s and MA104-GCaMP6s-IP_3R-TKO clones after
664 agonist screening using ADP and AC55541 (PAR2 agonist). **C.** (Left) MA104-GCaMP6s and
665 MA104-GCaMP6s-IP_3R-TKO cells before and after treatment with ADP. Traces (middle) and
666 quantitation (right) of GCaMP6s fluorescence showing Ca^{2+} responses of parental and IP_3R-KO
667 cells upon ADP addition (arrow). **D.** Agonist treatment studies as in (**C**) but using 0.75 μM
668 AC55541. **E.** MA104-GCaMP6s and MA104-GCaMP6s-IP_3R-TKO cells before and after 1 μM

669 thapsigargin treatment. Ca^{2+} signaling traces and quantitation showing normalized GCaMP6s
670 fluorescence after 1 μM thapsigargin treatment (arrow). **F.** Genomic DNA sequencing of IP_3R1,
671 IP_3R2, and IP_3R3 gRNA sites for MA104-GCaMP6s and MA104-GCaMP6s-IP_3R-TKO cells. All
672 data represented as mean ± SD. Statistical analyses were performed by Mann-Whitney test with
673 *p<0.05, ***p<0.001, ****p<0.0001. Scale bars are 50 μm.

674

675 **Figure 3.** Characterization of MA104-GCaMP6s and MA104-GCaMP6s-IP_3R-TKO cells (IP_3R-
676 TKO) during RV infection. **A.** Filmstrip images of RV infected MA104-GCaMP6s cells (white
677 outline, top row) and MA104-GCaMP6s-IP_3R-TKO cells (white outline, bottom row) overtime. **B.**
678 Four representative single-cell traces of normalized GCaMP6s fluorescence (F/F_0) from mock
679 (black) or RV-infected MA104-GCaMP6s cells (red) or MA104-GCaMP6s-IP_3R-TKO cells
680 (maroon) Arrows indicate example occurrences of an intercellular Ca^{2+} wave signal. **C.**
681 Quantitation of the number of Ca^{2+} spikes per cell in mock (grey), RV-infected and neighboring
682 cells for MA104-GCaMP6s and MA104-GCaMP6s-IP_3R-TKO cells. **D.** Maximum change in
683 normalized GCaMP6s fluorescence after supernatant transfer of RV infected MA104-GCaMP6s
684 (red) and MA104-GCaMP6s-IP_3R-TKO (blue) cells to MA104-GCaMP6s sensor cells treated
685 with 10μM BPTU. All data are shown as the mean ± SD. Statistical analyses were performed
686 using Kruskal-Wallis with Dunn's multiple corrections tests with ***p<0.001 & ****p<0.0001.
687 Scale bars are 50 μm.

688

689 **Figure 4.** Characterization of rotavirus infectivity and replication in MA104-GCaMP6s-IP_3R-TKO
690 cells. **A.** Representative images and diameter quantitation of RV plaques formed on MA104-
691 GCaMP6s or MA104-GCaMP6s-IP_3R-TKO cells. **B.** Quantitation of rotavirus infectivity by FFA
692 on MA104-GCaMP6s (red) or MA104-GCaMP6s-IP_3R-TKO (dark red) cells. **C.** One-step

693 rotavirus yield from MA104-GCaMP6s (red) or MA104-GCaMP6s-IP_3R-TKO (dark red) cells was
694 measured by plaque assay and graphed as Log_{10} plaque forming units (PFU) per cell. **D.** Kinetics
695 of rotavirus protein expression in MA104-GCaMP6s and MA104-GCaMP6s-IP_3R-TKO cells was
696 determined by immunoblot for GAPDH (top), NSP4 (middle), and a rabbit anti-rotavirus (strain
697 Alabama) (bottom). **E.** Immunofluorescence of RV-infected MA104-GCaMP6s and MA104-
698 GCaMP6s-IP_3R-TKO cells to detect NSP4 (blue) and NSP5 (magenta), as a marker of
699 viroplasms. All data are shown as the mean ± SD. Statistical analyses were performed using
700 Mann-Whitney T tests with *$p<0.05$ & ****$p<0.0001$. Scale bars are 20 μm.

701

702 **Figure 5.** Loss of IP_3R reduces rotavirus spread. **A.** Visualization of SA11-mRuby in plaques
703 from MA104-GCaMP6s or MA104-GCaMP6s-IP_3R-TKO cells. Brightfield (left) and SA11-mRuby
704 fluorescence (middle) images are merged on the right. Images were acquired with a Plan Fluor
705 objective (NA 0.30) with 10x10mm stich parameters. Scale bars are 1000 μm **B.** SA11-mRuby
706 spread in MA104-GCaMP6s (red) or MA104-GCaMP6s-IP_3R-TKO (blue) cells. Brightfield and
707 fluorescence (SA11-mRuby) images were acquired at the indicated times post infection using a
708 20x Plan Fluor objective (NA 0.45). **C.** SA11-mRuby yield from 24-96 hpi from MA104-GCaMP6s
709 (red) or MA104-GCaMP6s-IP_3R-TKO cells (blue) was measured by plaque assay and graphed
710 as Log_{10} PFU/mL. **D.** Live imaging of SA11-mRuby (RFP) spread in GCaMP6s-expressing
711 parental MA104-GCaMP6s (top) or MA104-GCaMP6s-IP_3R-TKO cells (bottom) from ~30-45 hpi.
712 All data are shown as the mean ± SD. Scale bars are 50 μm in B & D. **$p<0.01$ by T-test.

713

714 **Figure 6.** Blocking P2Y1-mediated ICWs reduces rotavirus plaque size. **A.** Representative
715 image of RV plaques formed on parental MA104 cell monolayers treated with DMSO (Top) or 1
716 μM BPTU (bottom). **B.** Measurement of plaque diameter for DMSO and 1 μM BPTU treated

717 cells. Data are shown as the mean ± SD. ***p<0.001 by Mann-Whitney T test.

718

719 **Figure 7.** P2Y1 Ca^{2+} signaling in LLC-MK2 cells. **A.** Ca^{2+} spikes per cell in mock (black),
720 rotavirus-infected (blue), and neighboring (NB3) uninfected (light blue) cells. ****p<0.0001 by
721 Kruskal-Wallis with Dunn's multiple corrections. **B.** Representative images of LLC-MK2 cell
722 monolayers before (top) and after (bottom) treatment with 25 nM ADP. **C.** Representative images
723 of LLC-MK2 and LLC-MK2+P2Y1 cell monolayers before (left) or after (right) agonist treatment
724 with 25nM ADP. **D.** Ca^{2+} signaling traces of LLC-MK2 (blue line) and LLC-MK2+P2Y1 cells
725 (purple line) after treatment with 25 nM ADP (arrow). **E.** P2Y purinergic receptor mRNA
726 expression by qPCR in LLC-MK2 and LLC-MK2+P2Y1 cells. Data were normalized to 18s
727 mRNA and plotted relative to P2Y12 mRNA transcript levels. ***p<0.0001 by individual T tests.
728 All data represented as mean ± SD. Scale bars are all 50 μm.

729

730 **Figure 8.** Reconstituting ICWs in LLC-MK2+P2Y1 cells increases rotavirus spread. **A.** Filmstrip
731 images of RV ICWs in LLC-MK2+P2Y1 cells. Scale bar is 50 μm. **B.** Ca^{2+} spikes per cell in
732 mock or RV infected and neighboring (NB3) LLC-MK2 cells. ***p<0.001 by Kruskal-Wallis with
733 Dunn's multiple correction test. **C.** Representative images of RV plaques formed on LLC-MK2
734 (Top) and LLC-MK2+P2Y1 (bottom) monolayers. **D.** RV infected (red) LLC-MK2 (left) and LLC-
735 MK2+P2Y1 (right) cell monolayers. White circles designate the margins of RV foci. Images
736 were captured using a Plan Fluor 10x objective (NA 0.30) with 15 x15 mm stich parameters. In
737 these stitched images, the scale bar represents 2000 μm. **E.** Quantitation of mean
738 fluorescence intensity of TRITC channel. *p<0.05 by Mann-Whitney T-test. All data are shown
739 as the mean ± SD.

740 **Table 1.** African green monkey IP_3R1, IP_3R2, and IP_3R3 gRNA sequences and exon target
741 sites.

Gene	Species	gRNA sequence (5')	gRNA target
IP_3R1	*Chlorocebus pygerythrus*	GCTGGATGACATCGTTCGCGTGG	exon 33
IP_3R2	*Chlorocebus pygerythrus*	CCACATGCACGTTGACCGGGATC	exon 19
IP_3R3	*Chlorocebus pygerythrus*	GTGCCCCATGAACCGCTACTCGG	exon 3

742

743 **Table 2.** African green monkey IP_3R1, IP_3R2, and IP_3R3 sequencing primers.

Gene	Species	Forward Sequence (5')	Reverse Sequence (5')
IP_3R1	*Chlorocebus pygerythrus*	TTTTTAGGGCCCGTGTGGTA	TTCATTCAGGTCGCATCCCC
IP_3R2	*Chlorocebus pygerythrus*	GAACTGAATGGGGCGAAACCT	TCTTCAACAAATTCCATTGTCAGG
IP_3R3	*Chlorocebus pygerythrus*	TCCAACTCCTGCCTCCTTTG	CACTGTCTCCACAAGCCACT

744

745 Table 3. Quantitative PCR primer sequences

Gene	Forward Sequence (5')	Reverse Sequence (5')
18s	GATATGCTCATGTGGTGTTG	AATCTTCTTCAGTCGCTCCA
P2Y1	CGTGCTGGTGTGGCTCATT	GGACCCCGGTACCTGAGTAGA
P2Y2	GAACTGACATGCAGAGGATAGAAGAT	GCCGGCGTGGACTCTGT
P2Y4	CCGTCCTGTGCCATGACA	TGACCGCCGAGCTGAAGT
P2Y6	GCCGGCGACCACATGA	GACCCTGCCTCTGCCATTT
P2Y11	CTGGAGCGCTTCCTCTTCAC	GGTAGCGGTTGAGGCTGATG
P2Y12	AGGTCCTCTTCCCACTGCTCTA	CATCGCCAGGCCATTTGT
P2Y14	TTCCTTTCAAGATCCTTGGTGACT	GCAGAGACCCTGCACACAAA

746

747

748 REFERENCES CITED

749

750 1. Berridge MJ. 2012. Calcium signalling remodelling and disease. Biochem Soc Trans 40:297-
751 309.
752 2. Zhou Y, Frey TK, Yang JJ. 2009. Viral calciomics: interplays between Ca2+ and virus. Cell
753 Calcium 46:1-17.
754 3. Hyser JM, Estes MK. 2015. Pathophysiological Consequences of Calcium-Conducting
755 Viroporins. Annu Rev Virol 2:473-96.
756 4. Michelangeli F, Ruiz MC, del Castillo JR, Ludert JE, Liprandi F. 1991. Effect of rotavirus
757 infection on intracellular calcium homeostasis in cultured cells. Virology 181:520-7.
758 5. Tian P, Estes MK, Hu Y, Ball JM, Zeng CQ, Schilling WP. 1995. The rotavirus nonstructural
759 glycoprotein NSP4 mobilizes Ca2+ from the endoplasmic reticulum. J Virol 69:5763-72.
760 6. Berkova Z, Morris AP, Estes MK. 2003. Cytoplasmic calcium measurement in rotavirus
761 enterotoxin-enhanced green fluorescent protein (NSP4-EGFP) expressing cells loaded with
762 Fura-2. Cell Calcium 34:55-68.
763 7. Zambrano JL, Diaz Y, Pena F, Vizzi E, Ruiz MC, Michelangeli F, Liprandi F, Ludert JE. 2008.
764 Silencing of rotavirus NSP4 or VP7 expression reduces alterations in Ca2+ homeostasis
765 induced by infection of cultured cells. J Virol 82:5815-24.
766 8. Ericson BL, Graham DY, Mason BB, Estes MK. 1982. Identification, synthesis, and
767 modifications of simian rotavirus SA11 polypeptides in infected cells. J Virol 42:825-39.
768 9. Sastri NP, Crawford SE, Estes MK. 2016. Pleiotropic Properties of Rotavirus Nonstructrual
769 Protein 4 (NSP4) and their Effects on Viral Replication and Pathogenesis, p 145-174. *In*
770 Svensson L, Desselberger U, Greenberg HB, Estes MK (ed), Viral Gastroenteritis: Molecular
771 Epidemiology and Pathogenesis. Elsevier Academic Press, Amsterdam.
772 10. Hyser JM, Collinson-Pautz MR, Utama B, Estes MK. 2010. Rotavirus disrupts calcium
773 homeostasis by NSP4 viroporin activity. mBio 1:e00265-10.
774 11. Pham T, Perry JL, Dosey TL, Delcour AH, Hyser JM. 2017. The Rotavirus NSP4 Viroporin
775 Domain is a Calcium-conducting Ion Channel. Sci Rep 7:43487.
776 12. Crawford SE, Hyser JM, Utama B, Estes MK. 2012. Autophagy hijacked through viroporin-
777 activated calcium/calmodulin-dependent kinase kinase-beta signaling is required for rotavirus
778 replication. Proc Natl Acad Sci U S A 109:E3405-E3413.
779 13. Crawford SE, Criglar JM, Liu Z, Broughman JR, Estes MK. 2019. COPII Vesicle Transport Is
780 Required for Rotavirus NSP4 Interaction with the Autophagy Protein LC3 II and Trafficking to
781 Viroplasms. J Virol 94.
782 14. Foskett JK, White C, Cheung KH, Mak DO. 2007. Inositol trisphosphate receptor Ca2+ release
783 channels. Physiol Rev 87:593-658.
784 15. Lock JT, Alzayady KJ, Yule DI, Parker I. 2018. All three IP3 receptor isoforms generate Ca(2+)
785 puffs that display similar characteristics. Sci Signal 11.
786 16. Foskett JK, Daniel Mak DO. 2010. Regulation of IP(3)R Channel Gating by Ca(2+) and Ca(2+)
787 Binding Proteins. Curr Top Membr 66:235-72.
788 17. Chang-Graham AL, Perry JL, Engevik MA, Engevik KA, Scribano FJ, Gebert JT, Danhof HA,
789 Nelson JC, Kellen JS, Strtak AC, Sastri NP, Estes MK, Britton RA, Versalovic J, Hyser JM.
790 2020. Rotavirus induces intercellular calcium waves through ADP signaling. Science 370.
791 18. Ando H, Hirose M, Mikoshiba K. 2018. Aberrant IP(3) receptor activities revealed by
792 comprehensive analysis of pathological mutations causing spinocerebellar ataxia 29. Proc Natl
793 Acad Sci U S A 115:12259-12264.
794 19. Lung O, Candlish R, Nebroski M, Kruckiewicz P, Buchanan C, Moniwa M. 2021. High-
795 throughput sequencing for species authentication and contamination detection of 63 cell lines.
796 Sci Rep 11:21657.
797 20. Chang-Graham AL, Perry JL, Strtak AC, Ramachandran NK, Criglar JM, Philip AA, Patton JT,
798 Estes MK, Hyser JM. 2019. Rotavirus Calcium Dysregulation Manifests as Dynamic Calcium
799 Signaling in the Cytoplasm and Endoplasmic Reticulum. Sci Rep 9:10822.

800 21. Perry JL, Ramachandran NK, Utama B, Hyser JM. 2015. Use of genetically-encoded calcium
801 indicators for live cell calcium imaging and localization in virus-infected cells. Methods 90:28-38.
802 22. Strtak AC, Perry JL, Sharp MN, Chang-Graham AL, Farkas T, Hyser JM. 2019. Recovirus NS1-
803 2 Has Viroporin Activity That Induces Aberrant Cellular Calcium Signaling To Facilitate Virus
804 Replication. mSphere 4.
805 23. Philip AA, Dai J, Katen SP, Patton JT. 2020. Simplified Reverse Genetics Method to Recover
806 Recombinant Rotaviruses Expressing Reporter Proteins. J Vis Exp doi:10.3791/61039.
807 24. Hyser JM, Zeng CQ, Beharry Z, Palzkill T, Estes MK. 2008. Epitope mapping and use of
808 epitope-specific antisera to characterize the VP5* binding site in rotavirus SA11 NSP4. Virology
809 373:211-228.
810 25. Criglar JM, Hu L, Crawford SE, Hyser JM, Broughman JR, Prasad BV, Estes MK. 2014. A novel
811 form of rotavirus NSP2 and phosphorylation-dependent NSP2-NSP5 interactions are associated
812 with viroplasm assembly. J Virol 88:786-98.
813 26. Maynard JP, Lee JS, Sohn BH, Yu X, Lopez-Terrada D, Finegold MJ, Goss JA, Thevananther
814 S. 2015. P2X3 purinergic receptor overexpression is associated with poor recurrence-free
815 survival in hepatocellular carcinoma patients. Oncotarget 6:41162-79.
816 27. Michelangeli F, Liprandi F, Chemello ME, Ciarlet M, Ruiz MC. 1995. Selective depletion of
817 stored calcium by thapsigargin blocks rotavirus maturation but not the cytopathic effect. J Virol
818 69:3838-3847.
819 28. Hyser JM, Utama B, Crawford SE, Broughman JR, Estes MK. 2013. Activation of the
820 endoplasmic reticulum calcium sensor STIM1 and store-operated calcium entry by rotavirus
821 requires NSP4 viroporin activity. J Virol 87:13579-88.
822 29. Ruiz MC, Cohen J, Michelangeli F. 2000. Role of Ca2+in the replication and pathogenesis of
823 rotavirus and other viral infections. Cell Calcium 28:137-49.
824 30. Berridge MJ, Lipp P, Bootman MD. 2000. The versatility and universality of calcium signalling.
825 Nat Rev Mol Cell Biol 1:11-21.
826 31. Ruiz MC, Aristimuno OC, Diaz Y, Pena F, Chemello ME, Rojas H, Ludert JE, Michelangeli F.
827 2007. Intracellular disassembly of infectious rotavirus particles by depletion of Ca2+
828 sequestered in the endoplasmic reticulum at the end of virus cycle. Virus Res 130:140-150.
829 32. Kania E, Roest G, Vervliet T, Parys JB, Bultynck G. 2017. IP(3) Receptor-Mediated Calcium
830 Signaling and Its Role in Autophagy in Cancer. Front Oncol 7:140.
831 33. Parys JB, Decuypere JP, Bultynck G. 2012. Role of the inositol 1,4,5-trisphosphate
832 receptor/Ca2+-release channel in autophagy. Cell Commun Signal 10:17.
833 34. Megha, Hasan G. 2017. Control of protein translation by IP(3)R-mediated Ca(2+) release in
834 Drosophila neuroendocrine cells. Fly (Austin) 11:0.
835 35. Zambrano JL, Sorondo O, Alcala A, Vizzi E, Diaz Y, Ruiz MC, Michelangeli F, Liprandi F, Ludert
836 JE. 2012. Rotavirus infection of cells in culture induces activation of RhoA and changes in the
837 actin and tubulin cytoskeleton. PLoS One 7:e47612.
838 36. Mitchell SJ, Rosenblatt J. 2021. Early mechanical selection of cell extrusion and extrusion
839 signaling in cancer. Curr Opin Cell Biol 72:36-40.
840 37. Rosenblatt J, Raff MC, Cramer LP. 2001. An epithelial cell destined for apoptosis signals its
841 neighbors to extrude it by an actin- and myosin-dependent mechanism. Curr Biol 11:1847-57.
842 38. Takeuchi Y, Narumi R, Akiyama R, Vitiello E, Shirai T, Tanimura N, Kuromiya K, Ishikawa S,
843 Kajita M, Tada M, Haraoka Y, Akieda Y, Ishitani T, Fujioka Y, Ohba Y, Yamada S, Hosokawa Y,
844 Toyama Y, Matsui T, Fujita Y. 2020. Calcium Wave Promotes Cell Extrusion. Curr Biol 30:670-
845 681 e6.
846 39. Wales P, Schuberth CE, Aufschnaiter R, Fels J, Garcia-Aguilar I, Janning A, Dlugos CP,
847 Schafer-Herte M, Klingner C, Walte M, Kuhlmann J, Menis E, Hockaday Kang L, Maier KC, Hou
848 W, Russo A, Higgs HN, Pavenstadt H, Vogl T, Roth J, Qualmann B, Kessels MM, Martin DE,
849 Mulder B, Wedlich-Soldner R. 2016. Calcium-mediated actin reset (CaAR) mediates acute cell
850 adaptations. Elife 5.

851